Fully Integrated Pitch-Matched AlScN PMUT-on-CMOS Array for High-Resolution Ultrasound Images

Eyglis Ledesma, Arantxa Uranga, Francesc Torres, and Núria Barniol, *Member, IEEE*

***Abstract*—This article presents a fully integrated pitch-matched piezoelectric micromachined ultrasonic transducers (PMUTs)-on-CMOS array with high potential in catheter-based ultrasound imaging systems and capabilities to obtain resolutions under 100 μm. The system-on-chip (SoC) consists of 7 × 7 AlScN PMUTs connected in a 1-D configuration where the six external rows are used to generate the acoustic pressure through three high-voltage (HV)-pulser CMOS circuits, and the central row is used to sense the incoming ultrasound wave which will be amplified by a low-noise amplifier (LNA) CMOS amplifier. The experimental verification in a liquid environment gave, as a first result, a peak frequency of 7.7 MHz with a normalized pressure (ST) of 1.98 kPa_{pp}*mm*V^{-1} and receiving sensitivity (SR) of 3.3 V/MPa, respectively, competitive sensitivities in comparison to the state-of-the-art. In the second part, ultrasonic imaging for different wires with a minimum diameter of 25 μm was demonstrated as expected from numerical simulations. The system's performance for ultrasound images was evaluated considering the product of the area and the resolution at 1 mm, giving competitive values compared with other reported ultrasound systems for catheter-based medical ultrasound imaging and the only one providing monolithic integration with the CMOS front-end circuitry.**

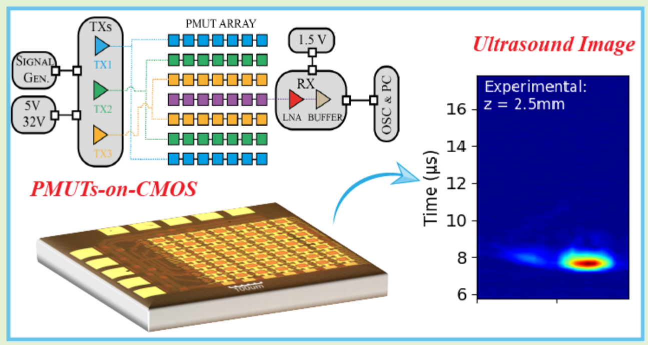

***Index Terms*—AlScN piezoelectric micromachined ultrasonic transducer (PMUT), catheter-based ultrasound systems, high resolution, PMUTs, PMUT-on-CMOS, ultrasound images.**

I. Introduction

ULTRASOUND-BASED medical diagnosis has become a useful tool for healthcare professionals to detect and evaluate several diseases. Catheter-based imaging, as intravascular ultrasound (IVUS) or intracardiac echocardiography (ICE), especially in cardiology and vascular surgery, requires a high resolution to evaluate the anatomy and detect lesions in the blood vessels. The lateral resolution in these systems can be determinant in certain aspects such as the evaluation of the thickness and composition of the arterial walls, or the detection and characterization of atherosclerotic plaques and as the presence of calcification, thrombi, and so on [1].

Manuscript received 7 March 2024; accepted 29 March 2024. Date of publication 11 April 2024; date of current version 15 May 2024. This work was supported in part by the Spanish Ministry of Science and Innovation under Project PID2019-108270RB-100 and Project PID2022-136624OB-10. The associate editor coordinating the review of this article and approving it for publication was Prof. Tsung-Heng Tsai.
(Corresponding author: Eyglis Ledesma.)
The authors are with the Department of Electronics Engineering, Universitat Autònoma de Barcelona, 08193 Bellaterra, Spain (e-mail: eyglis.ledesma@uab.cat; arantxa.uranga@uab.cat; francesc.torres@uab.cat; nuria.barniol@uab.cat).
Digital Object Identifier 10.1109/JSEN.2024.3385911

The fast development of microelectro-mechanical systems (MEMS) technology has aroused significant interest for this catheter-based ultrasound imaging systems. While ultrasound-based medical diagnosis has proven invaluable in detecting and evaluating various diseases, the advancement of MEMS technology holds particular promise in enhancing their capabilities, specifically providing robust fabrication processes for phased-array solid-state catheter-based probes [2], [3].

Commercial IVUS catheters have greatly advanced, offering detailed evaluations of blood vessels and plaque morphology [2], [4], [5], [6]. However, ongoing efforts within the scientific community have focused on improving catheter-based ultrasound devices, recognizing the importance of high-resolution ultrasound imaging. Traditional approaches, such as those using piezoelectric materials such as PZT in thickness mode resonance operation, have made significant contributions in ultrasound imaging [7], [8], [9], [10], [11], [12]. In 2018, Janjic et al. [7] presented a 2-D PZT-based forward-looking IVUS (FL-IVUS) to perform volumetric image. This system with a maximum diameter of 1.5 mm was able to achieve a good lateral resolution of 560 μm at a 6.5-mm penetration depth; however, its integration in small catheters continues to be a challenge.

A high-definition IVUS (HD-IVUS) system has also been studied to evaluate the influence of blood on the HD-IVUS image quality [10]. This system based on lithium niobate single crystal ($LiNbO_3$) in its thickness mode has a size of 0.6×0.8 mm^2 and a resonance frequency in water of 100.2 MHz, it achieves a lateral resolution of 324 μm by placing a 10-μm tungsten wire at 2.3 mm. As a final example of an IVUS system based on conventional piezoelectric transducers, in 2023 a novel dual-element was reported to improve the distortion suffering during the rotation of the catheter [11]. In this case, dual PZT elements with similar performance and frequency ($\sim$ 40 MHz) demonstrated their capability to resolve 10-μm wire imaging at approximately 246-μm axial distance with a lateral resolution of 167.3 and 184.6 μm for each piezoelectric element.

All these systems based on the conventional bulk ultrasound transducers face challenges such as: 1) complex fabrication processes for high-frequency devices in phased arrays, as well as combination with the front-end electronics with an application-specific integrated circuit (ASIC) and 2) need of matching layers to compensate for the mismatch between the acoustic impedances [2], [13]. Besides, note that PZT-based systems are lead-based, which in real medical scenarios could be dangerous to human health and should be replaced in the near future with more sustainable materials.

With respect to MEMS-based solutions, two different types of micromachined ultrasound transducers (MUTs) have been reported for catheter-based ultrasound imaging probes [3]: capacitive MUTs (CMUTs) [14], [15], [16], [17], [18], [19], [20] and piezoelectric micromachined ultrasonic transducers (PMUTs) [21], [22], [23]. Both are MEMS devices based on flexural membranes capable to produce and sense the ultrasound acoustic field by electrostatic actuation (CMUTs) or using a piezoelectrical layer as part of the membrane's layers (PMUTs). Both are microfabricated using robust microtechnology processes and offer distinct advantages. CMUTs, despite their requirement for high polarization voltages, demonstrate promise due to their small dimensions, compatibility with CMOS processes, and potential for high-density array fabrication. PMUTs, on the other hand, offer further advantages by eliminating the need for dc polarization voltages, simplifying the fabrication process (same element to transmit and receive) while maintaining the integration capabilities with CMOS circuitry [3], [24]. Some examples from the literature using CMUTs or PMUTs for phased-array systems are described here. In 2013 a 1-D CMUT array was designed to be implemented in an IVUS on guidewire, being determined to provide details about vessel dimensions, plaque composition, and so on. [14]. This system based on a 300×1000 μm CMUT array provides in water 277-μm lateral resolution at 2.4 mm with a frequency of 35.6 MHz. In 2020 [18], a highly integrated guidewire ultrasound imaging system-on-a-chip for vascular imaging was presented by the same group. It is based on a 1-D array of 12-element CMUTs working at 40 MHz in water and it is combined in a dedicated packaging with a complete front-end CMOS chip for transmission, reception, and signal processing of the ultrasound signals. The 12 elements consist of 40 square membranes with a 25-μm pitch (40×25 μm $= 1$ mm). The CMUTs array occupies an area smaller than $1 \times 0.3 = 0.3$ mm^2. Using a three 100-μm wires' phantom sample, an ultrasound image is demonstrated obtaining a 560-μm lateral resolution at 8 mm in the axial direction with a dc voltage bias of 44 V. Although the final idea is to achieve a system-on-chip (SoC), here the ultrasound transducer and ASIC are in separate chips, which increases the total area and affects the signal-to-noise ratio. On the other hand, in 2018, Pekař et al. [17] presented a 4-mm^2 1-D CMUT array of 32 circular CMUTs with 60-μm diameter, 65-μm pitch, wired to a front-end-specific CMOS chip inside a catheter for an intracardiac applications. The CMUTs can be operated at different frequencies depending on the imaging mode desired. In the resolution mode, where an image of a tissue-mimicking phantom was used, the CMUTs were operated at 20.8 MHz using a very large dc voltage bias (-160 V), providing a lateral resolution of 0.035 radians at a penetration depth of 16 mm.

Dealing with PMUTs, one of the first works for catheter-based systems, was presented in 2014 [23], where PZT was used as the piezoelectrical layer together with the silicon layer and the electrodes to form the flexural membrane. Two PMUT arrays with different-sized rectangular apertures were fabricated by bulk micromachining in silicon-on-insulator substrates. The PMUTs are rectangular shape with a dimension of 110×80 μm and operate at 5 MHz in water. The array containing 1024 PMUT membranes in 64×16 PMUTs (arranged in $64 \times 4 = 256$ elements) occupies an area 11.2×1.9 mm^2 and presents a theoretical lateral resolution of 1.1 mm at 4-cm penetration depth. Experimental data using this array demonstrated a lateral resolution of 1 mm at 3-cm penetration depth in an ultrasound image of a phantom tissue. In this work, the PMUTs were actuated and sensed by nonintegrated electronics. In 2019, Lee et al. [22] present a 6×6 pitch-matched 2-D PMUT array bonded to a specific integrated CMOS circuit with the electronics for ultrasound transmission and reception of the 36 channels. Each channel occupies 0.0625 mm^2 and is formed by four PMUTs with a pitch of 250 μm. The overall 36-channel 2-D array equals 2.25 mm^2. The PMUTs operate at 6 MHz in water. Using a phantom sample with three 500-μm diameter wires, they demonstrate ultrasound imaging using the PMUT and CMOS ASIC at different penetration depths, but the lateral resolution obtained is not quantified. An estimation of the lateral resolution can be done from the provided ultrasound image, giving approximately around 20° (equivalent to 8.7 mm) at a 25-mm penetration depth. Although this system presents a dedicated CMOS ASIC, it requires wafer bonding between the PMUT chip and the CMOS ASIC, which increases the complexity on the fabrication processing and can affect the signal-to-noise ratio. To our knowledge, there has not been yet any work presenting a PMUT system integrated with CMOS intended for catheter-based applications.

In this article, we present a novel pitch-matched PMUT-on-CMOS array tailored for low-dimensional catheter-based ultrasound systems. This integrated system has a small active area (430 $\times$ 430 μm) and a total area 0.46 mm^2 (including pads) conducive to easy integration inside small catheters with an area of 1 mm^2. In addition, the monolithic integration reduces the interconnection wires, improves the signal-to-noise ratio, and provides independence of the cable length between the PMUT receivers and the acquisition system. The significance of this work lies in its potential to achieve high lateral resolutions and detect targets smaller than half the wavelength, thus being the first step toward advancing the capabilities for catheter-based ultrasound imaging. The article structure contains two main sections and the conclusions. In Section II, the ultrasound system will be described considering performance and fabrication process. In Section III, experimental results including the characterization as an actuator and as a sensor as well as an ultrasound image demonstration will be presented and discussed.

II. Ultrasound System: Design and Fabrication

A. PMUT-on-CMOS Array Design

Ultrasound systems with narrow acoustic beams are essential to obtain ultrasound images with high resolutions. For catheter-based applications, probes with an outer diameter lower than 1.5 mm are required [7]. This means that the transducer area must be small enough to ensure that all the systems (transducers, pads, bonding connections, and so on) fit within the size of the catheter. The aperture of the transducer is directly related to the resolution of the system. For a PMUT array with focusing, lateral resolution or beamwidth at −6 dB, $BW_{-6\,dB}$, is defined by (1) where λ is the wavelength, and *F#* is the f_{number} defined as the ratio between focal length (F) and aperture of the array (L) [25]. Based on this expression, for a specific transducer (frequency and dimensions fixed) and acoustic medium, the only method to obtain narrow beams and, consequently improving the lateral resolution, will be decreasing the penetration depth or focal length. Furthermore, if a resolution of $\lambda/2$ is desired, *F#* should be equal to 0.5, which means that the target must be placed at $L/2$. This condition is challenging for small apertures. In a PMUT array, focusing is achieved electronically by simply applying the corresponding delays (electronic focusing) to different PMUT rows, allowing different focus with the same device and, increasing the transmission sensitivity when the focusing distance decreases [26]. In this sense and in comparison, with the use of fixed physical lens, different penetration depths, lateral resolutions, and acoustic pressures can be obtained in the same arrayed device with a simple modification of the applied waveform. Based on this, and considering our previous experience in high-frequency PMUT arrays [27], a PMUT array was chosen, with a total area of less than 1 mm^2, where the active area ($L \times L$) is 430 $\times$ 430 μm, and the dimensions considering all the pads are approximately 635 $\times$ 726 μm. With these dimensions, the theoretical lateral resolution at the natural focus (NF) of the PMUT array will be close to 100 μm, considering (1): $BW_{-6\,dB} = \lambda \cdot \mathrm{NF/L}$, and that the NF is given by the Rayleigh distance, $\mathrm{NF} = R_0 = \mathrm{Area}/(4\lambda) = L^2/(4\lambda)$. Moreover, sub-100-$\mu$m lateral resolution could be obtained using beamforming to focus at smaller penetration depths belonging to the near-field of the array

$$BW_{-6\,dB} \approx \lambda \cdot F\#. \tag{1}$$

B. PMUTs-on-CMOS Array Characteristics

The ultrasound system is based on a 1-D PMUT array fabricated monolithically on top of a 130-nm high-voltage (HV) CMOS analog front-end circuitry using the MEMS-on-CMOS process developed by Silterra [27], [33]. The array consists of 49 PMUTs arranged in seven rows connected through the top electrodes while the bottom electrode is common to all the systems. During the transmission of the ultrasound beam, the driving signals are generated by three HV CMOS transmitters based on a level-shifter topology generating 32-V pulses [34]. Each of the three TXs is applied at the top electrode of two rows configured symmetrically from the central row allowing focusing on the center along the axial direction. On the other hand, the received signal is amplified by a CMOS LNA which is directly connected to the central row making the PMUT-on-CMOS received signals independent of the length of cables to the acquisition system (in our case the oscilloscope). Here, low-voltage switches are not required which reduces the noise level (improving the signal-to-noise ratio and therefore the image quality) [35]. Besides, extra circuits are not necessary to produce the control signals, making the design and manufacturing process less complex and reducing the power consumption and area (if the electronic is on-chip). Finally, by avoiding switches the area is reduced facilitating the dimensional constraint to implement a pitch-matched system. The LNA presents a voltage–voltage gain of around 26 dB, a power consumption of 0.3 mW, and a bandwidth of 22 MHz [27]. The LNA amplifier is followed by a 50-Ω matched buffer, giving an overall reception area of 6 $\times$ 10^{-4} mm^2. Fig. 1 shows a diagram of the system where rows sharing the transmitter circuit are in the same color. This array arrangement with symmetry from the center is used to facilitate the beam focusing at different penetration depths. More complex configurations with TX/RX capabilities in each column will allow beam steering and beamforming for image reception enhancing the ultrasound image quality. These aspects are not included in this article.

Once the general system was presented, the single element in the array will be introduced. Each individual PMUT consists of a clamped multilayer membrane driven at its first out-of-plane flexural mode following the technological process described in [27] and [36]. The shape and size of the membrane are defined by the cavity, which in our case is a square of 40 $\times$ 40 μm. The multilayer membrane over the cavity is composed by a 0.6-μm piezoelectrical layer [AlN doped with 9.5 % of Sc ($Sc_{9.5\%}Al_{90.5\%}N$)], placed between two Al electrodes with thicknesses of 0.15 and 0.2 μm for the bottom and top electrodes, respectively. An etching step, through four external holes on the piezoelectric layer, allows the releasing of the membrane, defining the squared cavity with 600-nm height. Finally, a 1.5-μm thick Si_3N_4 layer is deposited by plasma-enhanced chemical vapor deposition (PECVD) process over all the PMUT structure. This layer acts as a passive

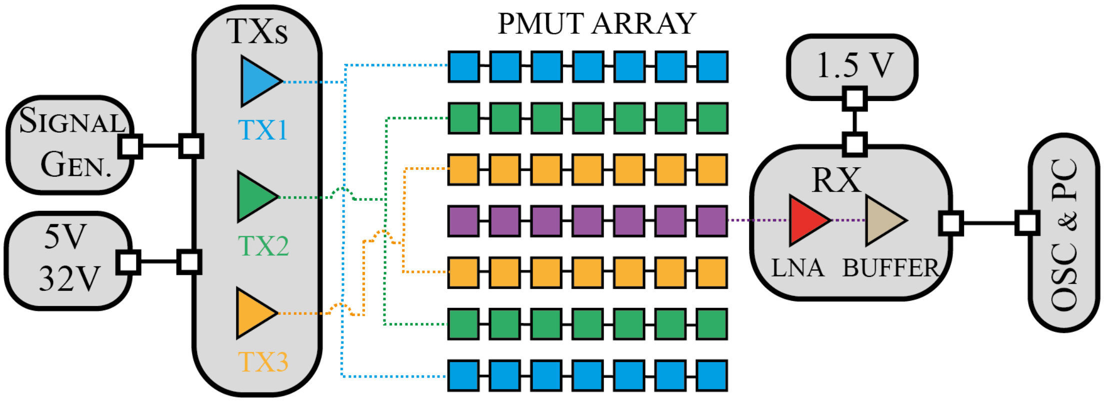

Fig. 1. General diagram of the ultrasound system based on a 1-D 7 × 7 PMUT array.

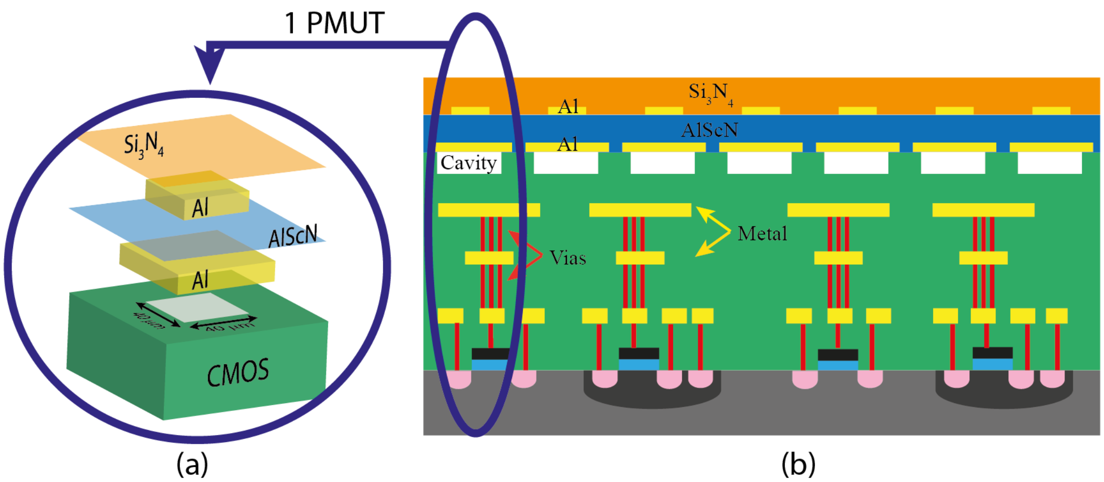

Fig. 2. (a) 3-D structure of a single PMUT-on-CMOS Silterra technology. (b) Cross section of one row of seven PMUTs-on-CMOS. In both the schematics layers are not to scale.

layer for promoting the flexural movement of the membrane and the sealing layer for the operation in liquid [see the 3-D structure of a single PMUT-on-CMOS in Fig. 2(a)]. Metal vias are used to interconnect the PMUT with the CMOS circuitry avoiding any bonding technique and decreasing the parasitic capacitance between PMUTs and CMOS circuitry. Fig. 2(b) shows a schematic layerś stack of one row of the PMUTs-on-CMOS array corresponding to seven single PMUTs.

Unlike conventional ultrasound transducers based on thickness mode, PMUTs work in the flexural mode where d_{31} piezoelectric coefficient creates a mechanical deformation via bending [39]. During the transmission (inverse piezoelectric effect), an ac signal between the top and bottom electrodes at the resonance frequency causes a deflection of the membrane and generates the acoustic wave. On the sensing mode (direct piezoelectric effect), the incoming ultrasound wave causes a vibration of the membrane which can be detected by measuring the electric output between both the electrodes. From the theoretical point of view, the resonance frequency for a PMUT device is described by (2a) where the value is determined by its physical characteristics: λ_{ij}^2 depends on the vibration mode, the shape, and the boundary conditions ($\lambda_{ij}^2 = 35.99$ for the first mode corresponding to a square clamped PMUT), a is the PMUT side, μ is the mass per unit area [see (2b)], and D is the flexural rigidity [see (2c)] [38], [39]. From these equations, t_n and ρ_n define the thickness and mass density of the nth layer, respectively; $E_{11,n}$ is the plate modulus and h_n defines the location of the top of each layer relative to the bottom of the laminate

$$f_{\text{air}} = \frac{\lambda_{ij}^2}{2\pi a^2}\sqrt{\frac{D}{\mu}}, \quad i = 1, 2, \ldots, \quad j = 1, 2, \ldots \tag{2a}$$

$$\mu_n = \sum_{n=1}^{N} t_n * \rho_n \tag{2b}$$

$$D \approx \frac{1}{3} * \sum_{n=1}^{N} E'_{11,n} * (\overline{h_n}^3 - \overline{h_{n-1}}^3). \tag{2c}$$

According to these analytical equations, the resulting multilayer single PMUT will be resonating at its first out-of-plane flexural movement with an expected frequency of 19.4 MHz in air. This frequency is closed to the obtained with the real PMUTs layout using FEM simulations in COMSOL, 20.6 MHz. Compared with our previous system [36], by reducing the PMUT size by half, the resonance frequency increases (improving the axial and lateral resolutions) and is more challenging to design a pitch-matched PMUT-on-CMOS system. In addition, the use of 9.5% scandium-doped AlN ensures

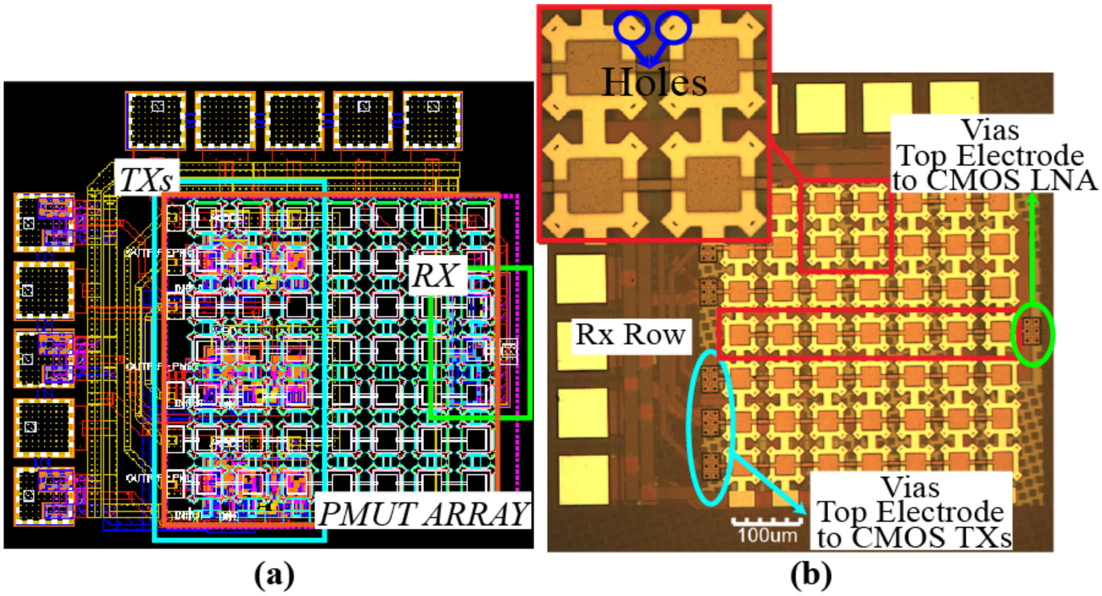

Fig. 3. (a) Layout and (b) optical image of the fabricated system. Inset: zoomed-in view to show the details of four PMUTs in the array.

better efficiency of the piezoelectric material regarding their capability to transform electrical energy in mechanics and vice versa, described by the electromechanical coupling factor K_t^2 [40], [41]. This figure-of-merit is directly related to $e_{31,f}^2/\epsilon_0{}^*\epsilon_r$ (where $e_{31,f}$ is the effective piezoelectric coefficient, ϵ_r is the relative permittivity, and ϵ_0 is the vacuum permittivity), giving 34.56 GPa for AlScN and 13.48 GPa for AlN, which is a 2.56× improvement due to Sc concentration of 9.5% [42].

The PMUT resonant frequency will be changed if the PMUT is operated in a fluid environment. In this case, the resonance frequency is affected by the medium properties which add an extra mass causing a drop in frequency; see (3) [45], [46]. This parameter is known as added virtual mass (β) and can be computed for a squared clamped device as shown in (4), which takes into account the fluid viscosity, η [47]. In the case of using Fluorinert (FC-70: c = 685 m/s, ρ = 1940 kg/m^3) as fluid medium, with a nonneglecting viscosity (η = 24 cP), this added virtual mass factor is β = 4.5, and in consequence, the resonance frequency in the liquid is expected at around 8.3 MHz

$$f_{\text{liquid}} = \frac{f_{\text{air}}}{\sqrt{1+\beta}} \tag{3}$$

$$\beta = 0.342\frac{\rho_{\text{liquid}} \cdot a}{\mu}\left(1 + 1.057\sqrt{\frac{\eta}{\rho_{\text{liquid}} \cdot a^2 \cdot \omega}}\right). \tag{4}$$

Fig. 3 illustrates the final layout and an optical image of the presented PMUTs-on-CMOS array where the pitch was set to 65 μm giving a fill factor of around 42%. The positions of the TXs and RX blocks shown in Fig. 1 have been highlighted [Fig. 3(a)] where all the CMOS circuitry is under the PMUT array, creating a complete and compact pitch-matched ultrasound system. Fig. 3(b) is an optical image of the PMUTs-on-CMOS array, highlighting the vias from the PMUT electrodes to the CMOS circuitry (which is placed underneath). The inset in Fig. 3(b) is a zoom on four PMUTs, to clearly show the four holes outside the cavity used for the releasing of the membrane and which are covered by the passive Si3N4 layer to guarantee watertightness.

III. Results and Discussion

A. Acoustic Characterization in a Liquid Environment

The acoustic tests of the PMUTs-on-CMOS ultrasound system were done with the array immersed in Fluorinert (FC-70: c = 685 m/s, ρ = 1940 kg/m^3). The system was bonded to a PCB using wedge–wedge wire bonding, the inputs of the transmitter circuits were connected to a signal generator (81150A, Keysight, USA), and the voltage signal at the LNA + buffer output was acquired by an oscilloscope (DSO-X 3054A, Keysight, USA). A 200-μm-diameter needle hydrophone from ONDA (HNC-0200, ONDA, USA) was used to measure the generated acoustic pressure.

1) Frequency Response: The frequency response of the system was obtained considering two scenarios. The first one is based on a pulse-echo configuration where the liquid–air interface was used as a reflecting surface. In this case, the transmitter rows were driven considering four unipolar pulses with 32 V of amplitude, and the frequency was modified from 5 to 20 MHz with a step of 250 kHz; see the setup in Fig. 4(a). The temporal responses at each frequency were acquired at three different times of flight corresponding to acoustic paths (APs) of 4, 6, and 8 mm (i.e., 2, 3, and 4 mm of FC-70 thickness, respectively) reaching a maximum amplitude of 70 mV when the AP is 4 mm and 15 mV when the distance traveled is double. Based on the obtained results, the peak frequency (f_0) appears at 7.7 MHz independently of the AP (or independently of the final liquid thickness). This frequency is close to the expected one computed in Section II (8.3 MHz) derived from the theoretical analysis (3). To corroborate these results, a second experiment was carried out by exciting the transmitter rows with one pulse of 65-ns width and computing the fast Fourier transform (FFT) from the echo acquired at 2 mm by the HNC-0200 hydrophone [see the setup in Fig. 4(a)]. Fig. 4(b) inset shows the results where

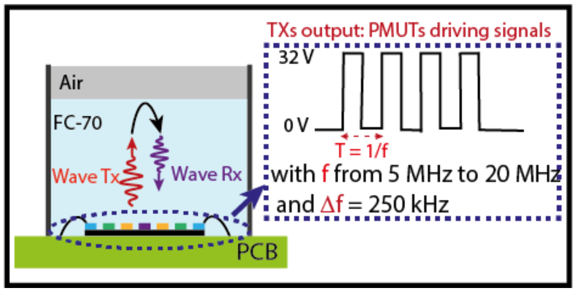

(a)

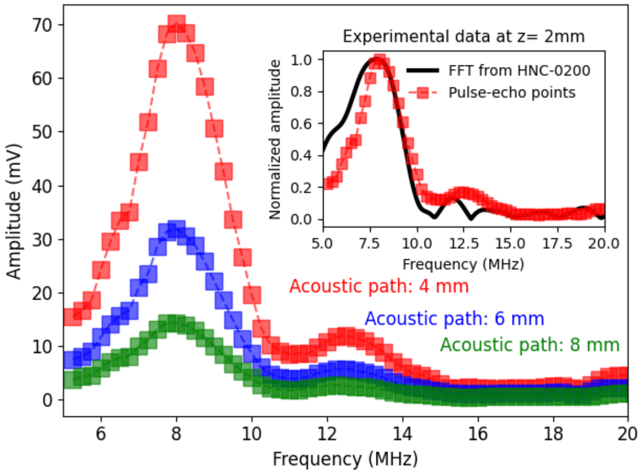

(b)

Fig. 4. (a) Experimental setup for the frequency characterization in Fluorinert (FC-70) in a pulse-echo configuration. The acquired signal by the oscilloscope is recorded for each of the actuation frequencies to determine the resonance frequency of the PMUTs-on-CMOS system. (b) Frequency response using a pulse-echo configuration at an AP of 4 mm (red squares), 6 mm (blue squares), and 8 mm (green squares). Inset: FFT corresponding to the hydrophone time response to a 65-ns pulse (solid black line) and the normalized pulse-echo response when the AP is 4 mm (red squares).

the solid black line corresponds to the FFT, and red squares correspond to the pulse-echo point at an AP of 4 mm, showing a good correspondence between them. Based on the FFT, the bandwidth at −6 dB is 3.9 MHz, which corresponds to a fractional bandwidth of around 50% (computed as bandwidth (@-6 dB)/f_0 *100).

2) Transmitting Sensitivity: The position in the plane and the axial distance was adjusted using a manual micro-positioner system to obtain the maximum pressure. All the transmitting rows were driven with four unipolar pulses at 7.7 MHz with 32-V amplitude. Electrical crosstalk is not expected in this case (see [26] for further details). Fig. 5(a) shows a schematic representation of the experimental setup.

The first acoustic measure was done after 3.6 μs corresponding to a distance between the hydrophone and the array surface of 2.5 mm. Fig. 5(b) inset shows the time response at this distance giving a peak-to-peak pressure of 29 kPa_{pp}. From this position, the hydrophone was lifted every 50 μm and the output pressure amplitudes were measured at each point; see red circles in Fig. 5(b). To obtain the pressure dependence with the distance ($A = P_0 * R_0$), the measured peak-to-peak values were fit according to the following expression [29], [43]:

$$P(z) = \frac{P_0 \cdot R_0}{z} e^{-\alpha z} = \frac{A}{z} e^{-\alpha z} \tag{5}$$

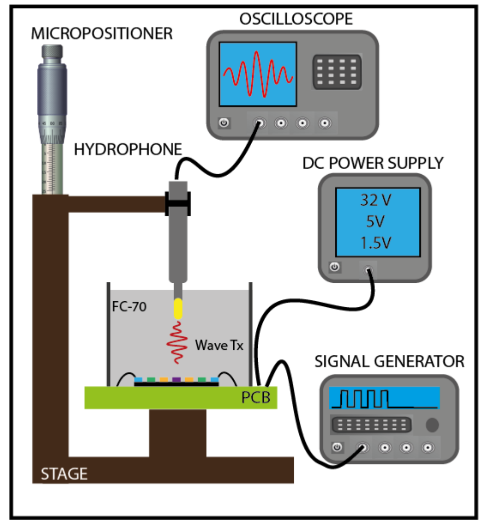

(a)

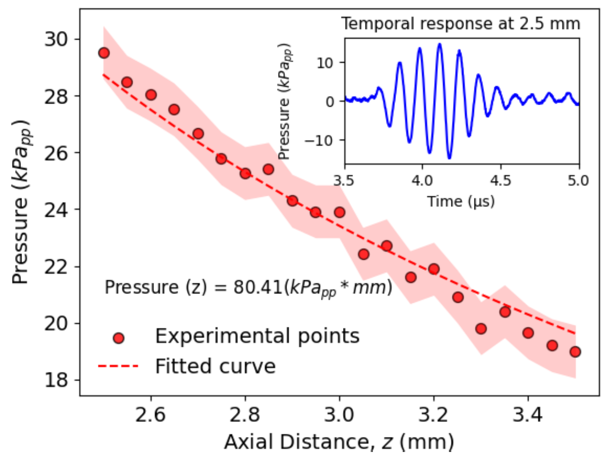

(b)

Fig. 5. Acoustic characterization as an actuator. (a) Schematic experimental setup. (b) Measured pressure at different heights from the array surface (red circles) and the fit curve (red dashed line), pink shadow corresponds to the experimental error. Inset: Temporal response at 2.5 mm.

where P_0 is the surface pressure, R_0 is the Rayleigh distance (R_0 = Transducer Surface$/4\lambda$), z is the axial distance, and α is the damping viscosity coefficient. The damping coefficient defined by (6) depends on the resonance frequency (f_0), the longitudinal or acoustic viscosity (η), the density (ρ), and the sound velocity (c) of the acoustic medium. Higher attenuation values are reached when the frequency is higher than 5 MHz [44], and it is important to estimate this parameter to obtain a better adjustment. Replacing all the terms considering FC-70 (c = 685 m/s, ρ = 1940 kg/m^3, η = 24 cP) and the resonance frequency of the PMUTs-on-CMOS array (f_0 = 7.7 MHz), the damping coefficient gives 45 m^{-1}

$$\alpha \approx \frac{2 \cdot \pi^2 \cdot f_0^2 \cdot \eta}{\rho \cdot c^3}. \tag{6}$$

Considering the damping coefficient and (5), the red dashed line in Fig. 5(b) shows the fit curve giving a pressure dependence of 80.41 $\text{kPa}_{\text{pp}} \cdot$ mm. Normalizing with the applied voltage and considering a factor of 1.27 due to the effective amplitude of a square signal in comparison to a sinusoidal one,

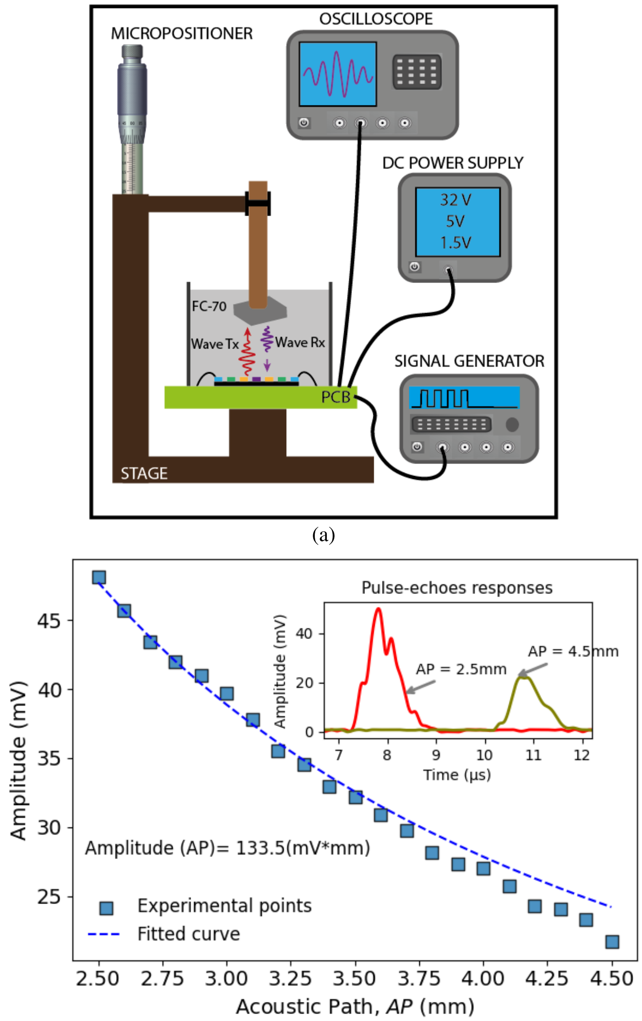

(b)

Fig. 6. Acoustic characterization as a sensor. (a) Schematic experimental setup. (b) Measured amplitude at different APs (blue square) and the fit curve (dashed blue line). Inset: Upper envelope of the received pulse-echo time response corresponding to two different APs, AP = 2.5 mm in red and AP = 4.5 mm in olive.

the ST obtained is 1.98 $\mathrm{kPa_{pp}} \cdot \mathrm{mm} \cdot \mathrm{V}^{-1}$. Taking into account this value and the active area (0.185 mm^2), the acoustic pressure from 1-mm^2 PMUT array area at 1.5 mm from its surface when 1 V is applied gives 7.1 $\mathrm{kPa_{pp}} \cdot \mathrm{mm}^{-2} \cdot \mathrm{V}^{-1}$.

3) Receiving Sensitivity: The receiving sensitivity (SR) was obtained by testing the system in a pulse-echo configuration. Here a metallic surface was used as a reflective surface and the position along the axial direction was modified giving an AP difference between every point of 100 μm; see Fig. 6(a). The transmitting rows were driven with four unipolar pulses at 7.7 MHz with 32-V amplitude, and the maximum value was acquired at each point. Fig. 6(b) (blue square) shows the measured amplitudes and the inset graph depicts the upper envelope in the first and last point. The results were fit taking into account the dependence of the amplitude with the AP and the losses due to the viscosity ($\alpha = 45\ \mathrm{m}^{-1}$), $\mathrm{V(AP)} = B/\mathrm{AP} * e^{-\alpha \mathrm{AP}}$, where the coefficient B gives 133.5 mV * mm; see dashed blue line in Fig. 6(b). The SR can be computed using $\mathrm{V(AP)}/(P(z)/2)$, where $P(z)$, obtained in the previous section (5), needs to be divided by 2 because this value refers to peak-to-peak pressure. Considering that, we obtained a sensitivity of 3.3 V/MPa.

4) Comparison With the State-of-the-Art: Table I shows a comparison of the presented PMUT-on-CMOS array with other PMUT-based systems reported in the state-of-the-art. The normalization with the distance and the applied voltage (ST) was used to compare the generated pressure at the same distance by different ultrasound transducers no matter what size they are. However, this normalization does not include the area, which is determining for catheter applications, and because of this, the parameter ST was divided by the effective area of the transducer thus providing the acoustic output pressure of the PMUT area of 1 mm^2 to 1.5 mm of its surface when 1 V is applied ($\mathrm{kPa/mm^2/V}$). From this result (ST normalized), it can be seen how the PZT-based PMUTs achieve an improvement transmitting performance of 2.8× [48] as expected. Similar benefits have been presented recently comparing PZT PMUTs with AlScN (Sc at 15%) [49].

To estimate the best performance as an actuator and as a sensor, the product ST*SR was defined as figure-of-merit, considering in all the cases the ST at 1.5 mm. Based on these results, the proposed AlScN PMUTs-on-CMOS array achieves an improvement of almost a factor of 2 in comparison to the PZT array (the best reported result in the table) used for dynamic monitoring of the arterial walls [48]. Compared with our previous PMUTs-on-CMOS arrays [27], [36], it can be seen how this system with small dimensions can generate 3.6× more pressure, doubling the frequency and with a slight

TABLE I
COMPARISON OF SYSTEMS BASED ON PMUTS AS ACTUATORS AND SENSORS

Parameters	2022[48]	2022[50]	2022[36]	This work
Total of PMUTs	1x12	5x17	7x7	7x7
Area (mm x mm//mm^2)	0.085x1.5// 0.128	0.31x1.99// 0.62[6]	0.71x0.71// 0.5	0.43x0.43// 0.185
Piezoelectric	PZT	PZT	AlN	AlScN
Media	Water	FC-70	FC-70	FC-70
Frequency (MHz)	5	4	3.3	7.7
Input Voltage	10 V_{pp}	5V	32V square	32V square
Pressure (kPa)	4.8@4mm[4]	8@1mm	8.9@2.5mm	29@2.5mm
ST (kPa·mm/V)	3.84[5]	1.6	0.55[7]	1.98[7]
Normalized ST@1.5mm $(\mathrm{kPa/mm^2/V})^2$	20	1.72	1.65	7.14
SR (V/MPa)	0.87	x	2.9	3.3
Normalized ST*SR*10−3@ 1.5mm (mm^2)	17.4	x	4.8	23.6

[1]Computed as Pressure*distance/Input voltage.
[2]It gives the acoustic output pressure from 1 mm^2 PMUT area at 1.5 mm from its surface when 1 V is applied.
[3]The area is computed taking into account the number of elements, 60 μm diameter and 75 μm of pitch.
[4]Extracted pressure from Fig. 5 when 1 column is used applying 10 V_{pp} at 5 MHz.
[5]Computed considering the input voltage divided by 2 because the pressure refers to the maximum value.
[6]The area is computed taking into account the number of elements, 70 μm diameter and 120 μm of pitch.
[7]The input voltage was considered as 32*1.27 to take into account the increase in the energy due to square signal.

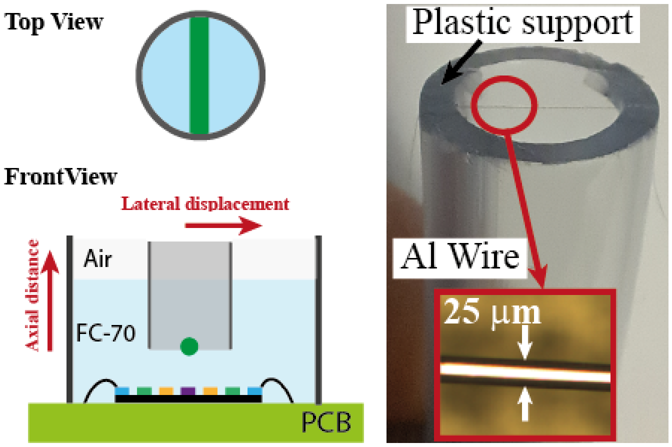

Fig. 7. Schematic and photograph of the phantom used to create the first ultrasound image.

increase in the SR than 7 × 7 AlN array (the size of a single PMUT is 80 μm) [36]. This is thanks to the change in the piezoelectric material from AlN to doped AlScN.

Likewise, with respect to the 7 × 7 AlScN array in [27] where the differences are given in the thicknesses of the layers (1-μm Si_3N_4, 0.4-μm bottom electrode, and 0.35-μm top electrode) [27], the normalized ST here (7.1 $kPa_{pp} * mm^{-2} * V^{-1}$) is 2.38× higher using one row less to transmit, as well as the sensed amplitude at 1 mm (133.5 mV) over the array surface increases in a factor of 5.8×.

B. Ultrasound Imaging

The ultrasound imaging demonstration and the capabilities of the PMUTs-on-CMOS array in terms of resolution were performed by carrying out a pulse-echo experiment using as a target a 25-μm Al wire. This wire was placed at three axial positions on top of the system (2.5, 3.5, and 4.8 mm, respectively) and was manually displaced 2 mm along the active aperture with a step of 100 μm; Fig. 7 shows the experimental setup.

For comparison, simulated ultrasound images were obtained using Field II considering the same experimental conditions. The resulting ultrasound images are shown in Fig. 8, where (a)–(c) corresponds to the simulation results and (d) and (e) shows the experimental ones. The ultrasound images were created by taking the temporal response (amplitude) at each lateral point (in steps of 100 μm). This temporal response was processed using a Hilbert transform to obtain the envelope, which was normalized regarding its maximum. Finally, all the results were plotted in a 2-D image where x-axis corresponds to the lateral distance and y-axis corresponds to the time. The measured results match with the image predicted by the simulations, demonstrating the PMUTs-on-CMOS ultrasound images' capabilities and the possibility of detecting targets with dimensions below 100 μm. Performing a cross section in a lateral direction at its maximum value, the obtained −6 dB beamwidth is 516, 649, and 926 μm for 2.5, 3.5, and 4.8 mm, respectively. To validate these values, (1) was used to compute the lateral resolution at the same positions, and we obtain at 2.5 mm a $BW_{-6\,dB} = 5.8\lambda = 517\ \mu m$; at 3.5 mm a $BW_{-6\,dB} = 8.1\lambda = 724\ \mu m$, and at 4.8 mm a $BW_{-6\,dB} = 11.2\lambda = 993\ \mu m$. The small beamwidth is obtained at the small distance, which implies that higher resolutions and then better quality in the image can be obtained at distances close to the array.

TABLE II
PROPERTIES AND DIMENSIONS OF THE WIRES USED IN ULTRASOUND IMAGING EXPERIMENT

Target ID	Diameter (μm)	Material
A	150	Copper with Insulation Coating Polyurethane
B	70	Copper
C	100	Tinned Copper
D	25	Aluminum

In the same context, a second ultrasound image experiment was carried out using four different wires as targets. The wires' diameter goes from 25 to 150 μm being made from different materials. Table II lists the properties of each one, and Fig. 9 bottom shows their optical images. The phantom was performed by fixing them in a plastic support side by side, and their axial position was slightly modified to obtain different times of flight and thus different start positions in the ultrasound image; see a schematic setup in Fig. 9 top. Such as in the previous experiment, the phantom was immersed in Fluorinert and a manual sweep with steps of 100 μm was carried out to displace the sample 9.3 mm.

Fig. 10 illustrates the final ultrasound image where all the wires are clearly identified as well as the liquid–air interface. Based on the time of flight, the thickness of the liquid is around 7.4 mm, and the interfaces were placed at 2.9, 3.9, 3.7, and 3.4 mm for A, B, C, and D, respectively. As in the previous experiment, the same distortion problem appears, for instance, the 150-μm wire gives a $BW_{-6\,dB} = 6.7\lambda = 600\ \mu m$ being four times greater than the real diameter. Besides, focusing on the incoming echo from interface B, the amplitude is very small in comparison to A and C (other copper interfaces, but bigger diameter) and even with D with a smaller diameter size. We attribute this effect to a change in the acoustic impedance of the B wire, which can be due to some oxidation of the copper wire. The peak-to-peak envelopes give a maximum value of around 4 mV_{pp} for the A interface and 2 mV_{pp} for the liquid–air interface.

1) Resolution Improvement: The previous ultrasound images demonstrated the capability to detect targets placed in a few millimeters' distance with dimensions in the micrometer range, arriving even at a size below 100 μm. Despite the good correspondence between the simulated and experimental results (see Fig. 8), it is true that the real size of the phantom (25 μm) is distorted, at least 20.6 times (516/25 μm where 516 μm corresponds to a cross section along the maximum value of the experimental image at 2.5 mm). Based on (1), it can be seen how if the target is placed at distances greater than the transducer aperture ($F > 5$L), the resolution increases in the same factor with respect to the wavelength ($BW_{-6\,dB} > 5\lambda$), being possible to reach a λ resolution if the transducer aperture and the focal distance have the same length. Considering the experimental data, the sound velocity in the acoustic medium (Fluorinert: c = 685 m/s), and the resonance frequency of the

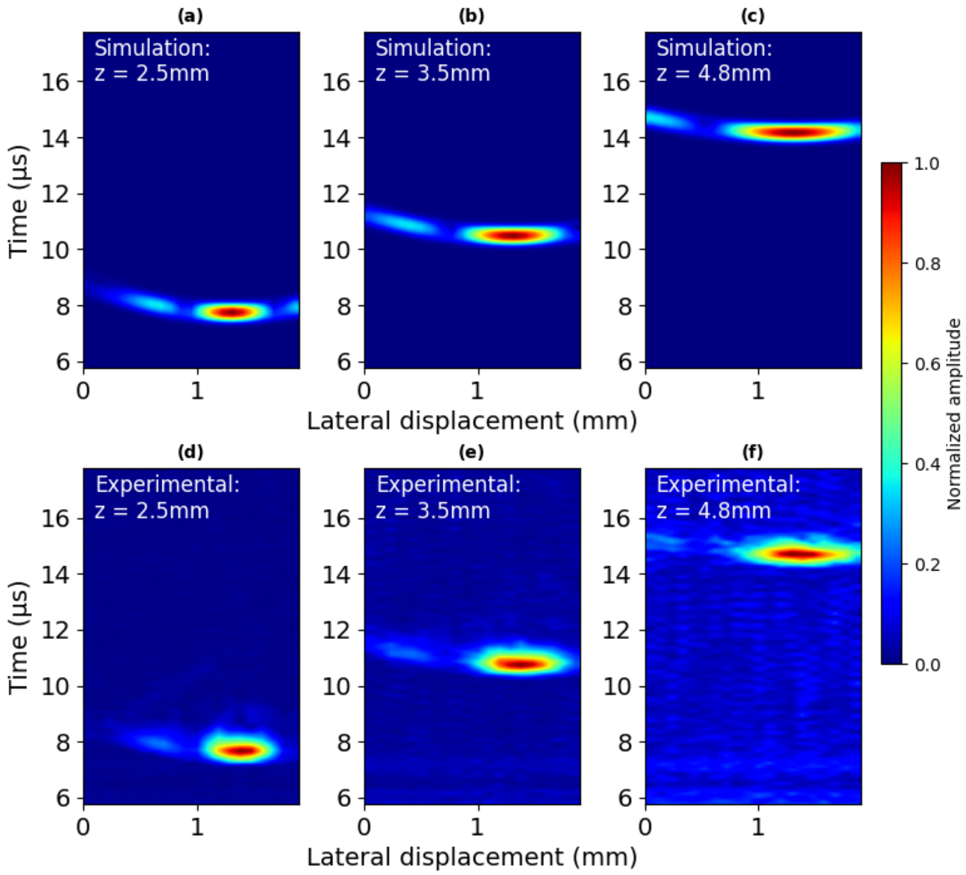

Fig. 8. Pulse-echo ultrasonic image of 25-μm Al wire placed at different axial positions, 2.5 mm (left), 3.5 mm (middle), and 4.8 mm (right). (a)–(c) Field II simulation. (d)–(f) Experimental points.

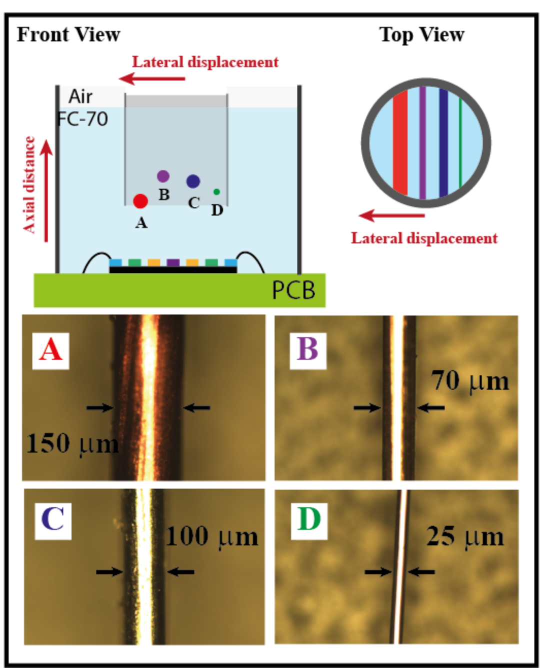

Fig. 9. Schematic illustration of the experimental setup for the pulse-echo ultrasonic image (top). Optical images of each used wires where the letters and colors correspond to their position in the plane (bottom).

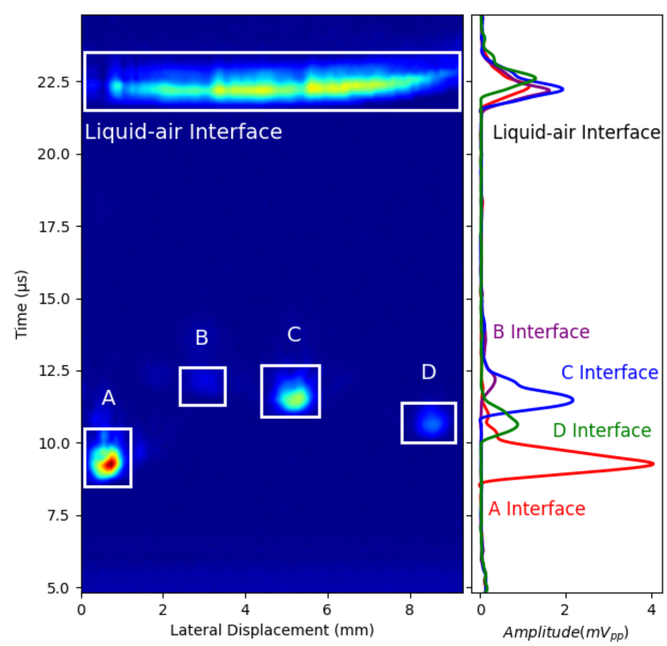

Fig. 10. Pulse-echo ultrasound image of four wires fixed in a plastic support and immersed in Fluorinert. Cross section along the time response placing the cut in the maximum of each interface (left). Red line: A target/wire; purple line: B wire; blue line: C wire; and green line: D wire.

system (7.7 MHz), the wavelength gives 89 μm which is a small value and could be interesting to achieve a resolution in this range for catheter-based ultrasound image applications. To obtain it, the target should be placed at 430 μm ($F = L$).

TABLE III
LATERAL RESOLUTION COMPARISON FROM DIFFERENT ULTRASOUND SYSTEMS

Ref.	Transducer kind, Material	CMOS Integration	Dimensions //area (A) (mm//mm^2)	Freq. (MHz)	Resolution@ AxialDistance (μm@mm)	Resolution@ 1mm (R') (μm)^a	R'· A (μm x mm^2)
2018 [7]	Bulk, PZT	No	Diam:1.5 //1.77	14	560@6.5	86	152.2
2022 [10]	Bulk, $LiNbO_3$	No	0.6x0.8 //0.48	100.2	324@2.3	141	67.7
2023 [11]	Bulk, PZT-5H	No	0.4x0.7 //0.28	40	167.3@0.246	680	190.4
2018 [17]	CMUT	No	2x2//4	20.8	0.035rad@16	35^b	140
2020 [18]	CMUT	Compatible// Chip bonded	1x0.3//0.3	40	560@8	70	21
2014 [23]	PMUT, PZT	No	1.1x6.3//6.93	5	1000@30	33.3	231
2019 [22]	PMUT(AlN)	Wafer bonded// Pitch matched	1.5x1.5//2.25	6	≈20°^{c}@25	≈349^{b,c}	≈785^c
This work	PMUT, AlScN	Monolithical/Pitch Matched	0.43x0.43 //0.185	7.7	480@2	240	44.4

^{a}Computed value using (1) where the experimental data were used to compute Resolution/AxialDistance and then, this ratio is multiplied by 1 mm.
^{b}Computed as the arc corresponding to the Resolution Angle at the AxialDistance: $R' = Angle \cdot AxialDistance \cdot 1mm/AxialDistance$.
^{c}Resolution estimated from experimental ultrasound image provided in [22].

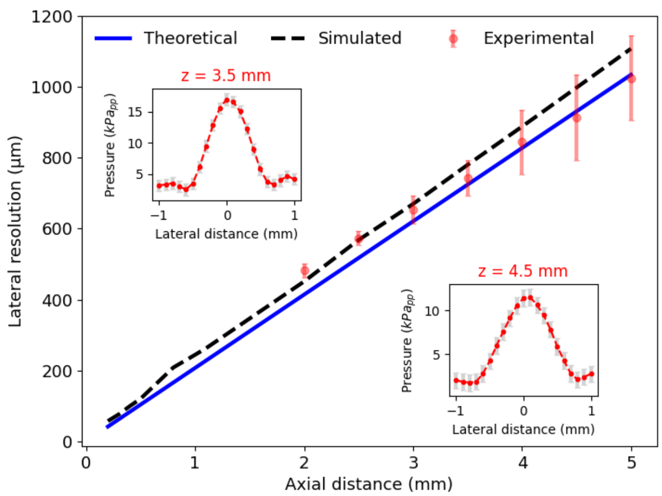

Fig. 11. Theoretical (blue solid line), simulated (dashed black line), and experimental (red circles) beamwidths versus axial distance. The inset images correspond to the experimental pressure distribution at 3.5-mm and 4.5-mm axial distances.

Due to our experimental setup, these distances are not reliable (bonding is not straight enough). As a consequence, a theoretical and simulated analysis was performed that was experimentally validated in the far-field regions.

Fig. 11 shows the theoretical (blue solid line), simulated (dashed black line), and experimental (red circles) beamwidths as a function of the axial position, where focusing techniques are required in the near-field.

The experimental points were obtained by displacing the HNC-0200 hydrophone along the active aperture from -1 mm to 1 mm with steps of 100 μm and acquiring the acoustic pressure at each point; see the inset graphs. From the inset images, as expected, at large axial distances, the beamwidth increases, and the maximum peak-to-peak pressure decreases. The minimum distance at which this hydrophone can be placed is 2 mm to not overestimate the beamwidth, and not underestimate the pressure [51], [52]. These results illustrate a good correlation with the measured beamwidth in simulation, and calculated analytically, allowing extrapolation of this behavior in the near-field, for instance, to obtain resolutions lower than 100 μm, the axial distance must be lower than 400 μm.

To demonstrate the resolution improvement in terms of ultrasound images, some simulations were performed in Field II. Fig. 12 illustrates the simulated normalized acoustic field from 100 μm to 5 mm along the axial direction and from -1 mm to 1 mm laterally without focusing (a), and focusing at 400 μm applying the corresponding delays (c). As it can be seen, when focusing techniques are used, the beamwidth decreases because the acoustic energy is concentrated in a narrow beam, improving the capability to detect objects with small dimensions. To validate it, the same 25-μm phantom was placed at 685 and 400 μm (electronic focusing was applied). The results are shown in Fig. 12(b) and (d); note that there is a clear improvement in lateral resolution when focusing techniques are used, and the phantom is placed at distances below 400 μm.

Table III presents a comparison from some state-of-the-art ultrasound systems designed for catheter applications. This comparison includes: systems based on thickness mode piezoelectrical transducers [7], [10], [11] and systems based on flexural membranes using MEMS-fabricated ultrasound transducers, either with CMUTs [17], [18] or with PMUTs [[22], [23], this work]. To provide a comparison between them, we normalize the lateral resolution which is provided by different axial positions for each of the systems, and based on (1), we recalculated them at the same axial distance (1 mm). In addition, a figure-of-merit (FoM = Resolution · Area) is defined to clearly obtain which system achieves the best resolution with the smallest size (i.e., FoM smaller), making the system more suitable for catheter applications. In Table III, we have also included a column explaining the capabilities to be integrated in CMOS technology. According to Table III, the smaller FoMs are obtained with systems based in MEMS fabrication processes: based on CMUTs [18] and the system presented here which is based on PMUTs. In addition, both the systems can be integrated with CMOS, although only our approach presents a monolithically integrated system. Finally, our system has the lowest operation frequency, which prevents for signal attenuation at large distance, improving the

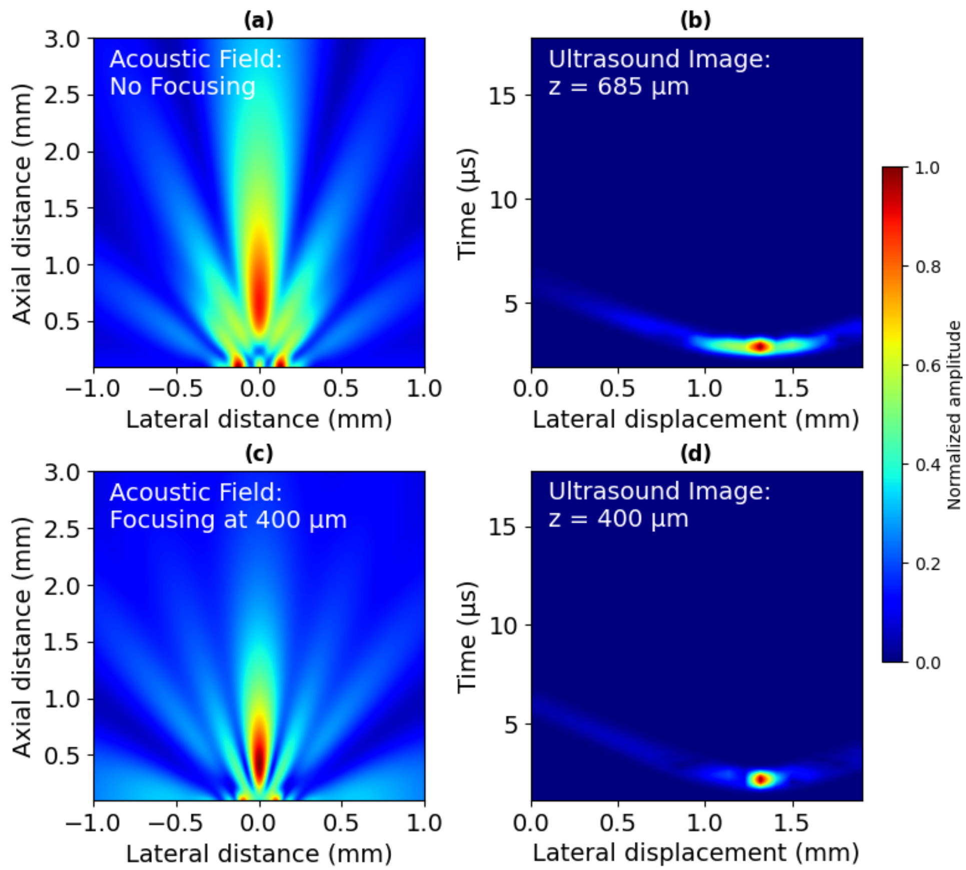

Fig. 12. Field II simulation results. Normalized pressure map (a) without focusing and (c) focusing at 400 μm. Pulse-echo ultrasonic image of a 25-μm Al wire placed at the corresponding focal points (maximum pressure points), at (b) 685 μm and (d) 400 μm.

signal-to-noise ratio and eventually the quality of the image. These results demonstrate the benefits of this tiny AlScN PMUT-on-CMOS array.

IV. Conclusion

In this article, the high resolution and IVUS imaging potential of an AlScN PMUTs-on-CMOS array with an area lower than 1 mm^2 is demonstrated. The system has been monolithically integrated with the CMOS analog front-end, achieving a pitch-matched system with high performance in terms of transmitted (1.98 kPa$_{pp}$*mm*V^{-1}) and sensed pressures (3.3 V/MPa) at 7.7 MHz in Fluorinert. Ultrasonic images of a target with dimensions less than $\lambda/2$ (wire diameter 25 μm) were successfully demonstrated, being a great achievement for the practical implementation of this system in small IVUS catheters. Likewise, a second experiment with targets with different diameters was carried out and checked the capabilities of the PMUTs-on-CMOS array in front of different sizes and materials. The defined figure of merit (R'·A) allows us to compare the capabilities of our system with the state-of-the-art to provide the best resolution with a very small area and monolithic CMOS integration. The use of PMUT arrays like this, as opposed to ultrasound systems with lens, offers a powerful tool for focusing at different points along the axial direction, achieving in this case, sub-100-μm resolutions for focusing distances less than 400 μm.

Acknowledgment

The authors would like to specifically acknowledge Eloi Marigó Ferrer and all the other members of the SilTerra's MEMS and SENSORS technology development team for supporting the fabrication of the PMUT-on-CMOS wafers.

References

[1] C. Zhu, L. Miao, K. Wei, D. Shi, and J. Gao, "Coronary microvascular dysfunction," *Microvascular Res.*, vol. 153, May 2024, Art. no. 104652.

[2] C. Peng, H. Wu, S. Kim, X. Dai, and X. Jiang, "Recent advances in transducers for intravascular ultrasound (IVUS) imaging," *Sensors*, vol. 21, no. 10, p. 3540, May 2021, doi: 10.3390/s21103540.

[3] E. Moisello, L. Novaresi, E. Sarkar, P. Malcovati, T. L. Costa, and E. Bonizzoni, "PMUT and CMUT devices for biomedical applications: A review," *IEEE Access*, vol. 12, pp. 18640–18657, 2024, doi: 10.1109/ACCESS.2024.3359906.

[4] Philips. *Visions PV.014P RX*. Accessed: Jul. 17, 2023. [Online]. Available: https://www.philips.es/healthcare/product/HCIGTD014R/visions-pv-014p-rx-digital-ivus-catheter

[5] Boston Scientific. *OptiCrossTM*. Accessed: Jul. 17, 2023. [Online]. Available: https://www.bostonscientific.com/es-ES/productos/sistemas-de-diagnostico-por-imagenes/cateter-para-toma-de-imagenes-coronarias-opticross.html

[6] ACIST. *HD IVUS Kodama*. Accessed: Jul. 17, 2023. [Online]. Available: https://acist.es/kodamahd-ivus-catheter/

[7] J. Janjic et al., "A 2-D ultrasound transducer with front-end ASIC and low cable count for 3-D forward-looking intravascular imaging: Performance and characterization," *IEEE Trans. Ultrason., Ferroelectr., Freq. Control*, vol. 65, no. 10, pp. 1832–1844, Oct. 2018.

[8] J. Lee, J.-Y. Moon, and J. Chang, "A 35 MHz/105 MHz dual-element focused transducer for intravascular ultrasound tissue imaging using the third harmonic," *Sensors*, vol. 18, no. 7, p. 2290, Jul. 2018.

[9] J. Hong et al., "A dual-mode imaging catheter for intravascular ultrasound application," *IEEE Trans. Med. Imag.*, vol. 38, no. 3, pp. 657–663, Mar. 2019.

[10] S. Liang et al., "Evaluation of blood induced influence for high-definition intravascular ultrasound (HD-IVUS)," *IEEE Trans. Ultrason., Ferroelectr., Freq. Control*, vol. 69, no. 1, pp. 98–105, Jan. 2022.

[11] B. Liu et al., "A novel dual-element catheter for improving non-uniform rotational distortion in intravascular ultrasound," *IEEE Trans. Biomed. Eng.*, vol. 70, no. 6, pp. 1768–1774, May 2023.

[12] Y. M. Hopf et al., "A pitch-matched high-frame-rate ultrasound imaging ASIC for catheter-based 3-D probes," *IEEE J. Solid-State Circuits*, vol. 59, no. 2, pp. 476–491, Feb. 2024.

[13] J. Jung, W. Lee, W. Kang, E. Shin, J. Ryu, and H. Choi, "Review of piezoelectric micromachined ultrasonic transducers and their applications," *J. Micromech. Microeng.*, vol. 27, no. 11, Nov. 2017, Art. no. 113001.

[14] T. Xu, C. Tekes, S. Satir, E. Arkan, M. Ghovanloo, and F. L. Degertekin, "Design, modeling and characterization of a 35 MHz 1-D CMUT phased array," in *Proc. IEEE Int. Ultrason. Symp. (IUS)*, Jul. 2013, pp. 1987–1990.

[15] J. Lim, C. Tekes, F. L. Degertekin, and M. Ghovanloo, "Towards a reduced-wire interface for CMUT-based intravascular ultrasound imaging systems," *IEEE Trans. Biomed. Circuits Syst.*, vol. 11, no. 2, pp. 400–410, Apr. 2017.

[16] D. Hah, C. H. Je, and S.-Q. Lee, "Design of capacitive micromachined ultrasonic transducers (CMUTs) on a flexible substrate for intravascular ultrasonography (IVUS) applications," in *Proc. Symp. Design, Test, Integr. Packag. MEMS/MOEMS (DTIP)*, May 2017, pp. 1–5.

[17] M. Pekař et al., "Quantitative imaging performance of frequency-tunable capacitive micromachined ultrasonic transducer array designed for intracardiac application: Phantom study," *Ultrasonics*, vol. 84, pp. 421–429, Mar. 2018.

[18] J. Lim, C. Tekes, E. F. Arkan, A. Rezvanitabar, F. L. Degertekin, and M. Ghovanloo, "Highly integrated guidewire ultrasound imaging system-on-a-chip," *IEEE J. Solid-State Circuits*, vol. 55, no. 5, pp. 1310–1323, May 2020.

[19] J. M. Rothberg et al., "Ultrasound-on-chip platform for medical imaging, analysis, and collective intelligence," *Proc. Nat. Acad. Sci. USA*, vol. 118, no. 27, p. 9, Jul. 2021, doi: 10.1073/pnas.2019339118.

[20] J. Wang, Z. Zheng, J. Chan, and J. T. W. Yeow, "Capacitive micromachined ultrasound transducers for intravascular ultrasound imaging," *Microsyst. Nanoeng.*, vol. 6, no. 1, p. 73, Aug. 2020, doi: 10.1038/s41378-020-0181-z.

[21] D. E. Dausch, J. B. Castellucci, D. R. Chou, and O. T. von Ramm, "5I-4 piezoelectric micromachined ultrasound transducer (pMUT) arrays for 3D imaging probes," in *Proc. IEEE Ultrason. Symp.*, Mar. 2006, pp. 934–937.

[22] J. Lee et al., "11.1 a 5.37 mW/Channel pitch-matched ultrasound ASIC with dynamic-bit-shared SAR ADC and 13.2 V charge-recycling TX in standard CMOS for intracardiac echocardiography," in *IEEE Int. Solid-State Circuits Conf. (ISSCC) Dig. Tech. Papers*, Feb. 2019, pp. 190–192.

[23] D. E. Dausch, K. H. Gilchrist, J. B. Carlson, S. D. Hall, J. B. Castellucci, and O. T. von Ramm, "In vivo real-time 3-D intracardiac echo using PMUT arrays," *IEEE Trans. Ultrason., Ferroelectr., Freq. Control*, vol. 61, no. 10, pp. 1754–1764, Oct. 2014.

[24] Y. Qiu et al., "Piezoelectric micromachined ultrasound transducer (PMUT) arrays for integrated sensing, actuation and imaging," *Sensors*, vol. 15, no. 4, pp. 8020–8041, Apr. 2015.

[25] J. Li and Z. Chen, "Integrated intravascular ultrasound and optical coherence tomography technology: A promising tool to identify vulnerable plaques," *J. Biomed. Photon. Eng.*, vol. 1, no. 4, pp. 209–224, 2015.

[26] E. Ledesma, I. Zamora, A. Uranga, and N. Barniol, "Multielement ring array based on minute size PMUTs for high acoustic pressure and tunable focus depth," *Sensors*, vol. 21, no. 14, p. 4786, Jul. 2021.

[27] I. Zamora, E. Ledesma, A. Uranga, and N. Barniol, "Phased array based on AlScN piezoelectric micromachined ultrasound transducers monolithically integrated on CMOS," *IEEE Electron Device Lett.*, vol. 43, no. 7, pp. 1113–1116, Jul. 2022.

[28] J. L. Butler and C. H. Sherman, *Transducers and Arrays for Underwater Sound*. New York, NY, USA: Springer, 2016.

[29] D. T. Blackstock, *Fundamentals of Physical Acoustics*. Hoboken, NJ, USA: Wiley, 2000.

[30] *3MTM Fluorinert TM Electronic Liquid FC-70 Product Description*, 3M Company, Minnesota, USA, 2019.

[31] J. A. Jensen and N. B. Svendsen, "Calculation of pressure fields from arbitrarily shaped, apodized, and excited ultrasound transducers," *IEEE Trans. Ultrason., Ferroelectr., Freq. Control*, vol. 39, no. 2, pp. 262–267, Mar. 1992.

[32] J. A. Jensen, "Field: A program for simulating ultrasound systems," *Med. Biol. Eng. Comput.*, vol. 34, no. 1, pp. 351–352, Jan. 1996.

[33] E. Ledesma, I. Zamora, J. Yanez, A. Uranga, and N. Barniol, "Single-cell system using monolithic PMUTs-on-CMOS to monitor fluid hydrodynamic properties," *Microsyst. Nanoeng.*, vol. 8, no. 1, p. 76, Jul. 2022.

[34] I. Zamora, E. Ledesma, A. Uranga, and N. Barniol, "Miniaturized 0.13-μm CMOS front-end analog for AlN PMUT arrays," *Sensors*, vol. 20, no. 4, p. 1205, Feb. 2020.

[35] I. Zamora, E. Ledesma, A. Uranga, and N. Barniol, "Monolithic single PMUT-on-CMOS ultrasound system with +17 dB SNR for imaging applications," *IEEE Access*, vol. 8, pp. 142785–142794, 2020.

[36] E. Ledesma, I. Zamora, A. Uranga, and N. Barniol, "A 0.5 mm^2 pitch-matched AlN PMUT-on-CMOS ultrasound imaging system," in *Proc. IEEE Int. Ultrason. Symp. (IUS)*, Oct. 2022, pp. 1–4.

[37] M. Soundara Pandian et al., "Thin film piezoelectric devices integrated on CMOS," in *Proc. Symp. Piezoelectricity, Acoustic Waves, Device Appl. (SPAWDA)*, Oct. 2016, pp. 167–170.

[38] R. D. Blevins, *Formulas for Natural Frequency and Mode Shape*. New York, NY, USA: Litton Educ. Publishing, 1979.

[39] D. Horsley, Y. Lu, and O. Rozen, "Flexural piezoelectric resonators," in *Piezoelectric MEMS Resonators*, H. Bhugra and G. Piazza, Eds. Cham, Switzerland: Springer, 2017, pp. 153–173.

[40] H. Bhugra and G. Piazza, *Piezoelectric MEMS Resonators*. Cham, Switzerland: Springer, 2017.

[41] R. Lu, M.-H. Li, Y. Yang, T. Manzaneque, and S. Gong, "Accurate extraction of large electromechanical coupling in piezoelectric MEMS resonators," *J. Microelectromech. Syst.*, vol. 28, no. 2, pp. 209–218, Apr. 2019.

[42] E. Ledesma, I. Zamora, A. Uranga, and N. Barniol, "9.5% scandium doped ALN PMUT compatible with pre-processed CMOS substrates," in *Proc. IEEE 34th Int. Conf. Micro Electro Mech. Syst. (MEMS)*, Jan. 2021, pp. 887–890.

[43] L. E. Kinsler, A. R. Frey, A. B. Coppens, and J. V. Sanders, *Fundamentals of Acoustics*, 4th ed. Hoboken, NJ, USA: Wiley, 2000.

[44] E. Kang et al., "A variable-gain low-noise transimpedance amplifier for miniature ultrasound probes," *IEEE J. Solid-State Circuits*, vol. 55, no. 12, pp. 3157–3168, Dec. 2020.

[45] M. Olfatnia, Z. Shen, J. M. Miao, L. S. Ong, T. Xu, and M. Ebrahimi, "Medium damping influences on the resonant frequency and quality factor of piezoelectric circular microdiaphragm sensors," *J. Micromech. Microeng.*, vol. 21, no. 4, Apr. 2011, Art. no. 045002.

[46] J. J. Bernstein et al., "Micromachined high frequency ferroelectric sonar transducers," *IEEE Trans. Ultrason., Ferroelectr., Freq. Control*, vol. 44, no. 5, pp. 960–969, Sep. 1997.

[47] Y. Kozlovsky, "Vibration of plates in contact with viscous fluid: Extension of Lamb's model," *J. Sound Vibrat.*, vol. 326, nos. 1–2, pp. 332–339, Sep. 2009.

[48] X. Jiang, V. Perrot, F. Varray, S. Bart, and P. G. Hartwell, "Piezoelectric micromachined ultrasonic transducer for arterial wall dynamics monitoring," *IEEE Trans. Ultrason., Ferroelectr., Freq. Control*, vol. 69, no. 1, pp. 291–298, Jan. 2022.

[49] A. S. Savoia et al., "Performance analysis of wideband PMUTs: A comparative study between sol-gel PZT, PVD PZT, and 15% ScAlN-based arrays through experimental evaluation," in *Proc. IEEE Int. Ultrason. Symp. (IUS)*, Sep. 2023, pp. 1–4.

[50] Z. Liu, S. Yoshida, D. A. Horsley, and S. Tanaka, "Fabrication and characterization of row-column addressed pMUT array with monocrystalline PZT thin film toward creating ultrasonic imager," *Sens. Actuators A, Phys.*, vol. 342, Aug. 2022, Art. no. 113666.

[51] R. A. Smith, "Are hydrophones of diameter 0.5 mm small enough to characterize diagnostic ultrasound equipment?" *Phys. Med. Biol.*, vol. 34, pp. 1607–1953, Jan. 1989.

[52] S. Umchid, "Spatial averaging correction for ultrasound hydrophone calibrations," *Int. J. Appl. Biomed. Eng.*, vol. 9, no. 1, pp. 33–38, 2016.

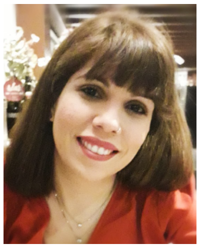

Eyglis Ledesma received the B.Sc. degree in telecommunication and electronic engineering from the Havana University of Technology José Antonio Echevarria, Havana, Cuba, in 2014, and the Ph.D. degree in electronic and telecommunications engineering from Universitat Autònoma de Barcelona, Bellaterra, Spain, in 2022.

She is a Postdoctoral Researcher with Universitat Autònoma de Barcelona. Her research interest includes piezoelectric microelectro-mechanical systems (MEMS) devices for ultrasonic sensor applications.

Arantxa Uranga received the degrees in physics and electronics engineering from Valladolid University, Valladolid, Spain, in 1994 and 1996, respectively, and the Ph.D. degree in electronics engineering from the Universitat Autònoma de Barcelona, Bellaterra, Spain, in 2001.

Since 1996, she has been with the Department of Electronics Engineering, Universitat Autònoma de Barcelona, where she is currently an Associate Professor. Her research interests include the design of CMOS circuits for RF processing and sensor applications, focusing on micro-electromechanical systems (MEMS)/NEMS devices.

Francesc Torres received the degree in physics and the Ph.D. degree in physics from the Universitat de Barcelona, Barcelona, Spain, in 1997 and 2001, respectively.

He has held three postdoctoral positions, with a focus on quantum computing for three years at the Instituto de Microelectrónica de Madrid IMM-CSIC of the Spanish Research Council, Madrid, Spain, magnetoplasmonic devices for seven months at IMM with a CSIC contract, and microelectro-mechanical systems (MEMS) devices at Universitat Autònoma de Barcelona (UAB), Bellaterra, Spain, for three years under a Spanish government contract "Juan de la Cierva." In addition, he held a five-year Spanish government contract "Ramon y Cajal," during which he worked on MEMS-NEMS at UAB. Currently, he holds an Associate Professor position at Universitat Autónoma de Barcelona, where he dedicates his efforts to the applications of MEMS-NEMS. His primary areas of focus include collaborative work on the design and fabrication of MEMS systems for energy harvesting and storage, exploring quantum phenomena associated with NEMS devices and researching ultrasound generation and imaging using piezoelectric micromachined ultrasonic transducers (PMUTs).

Núria Barniol (Member, IEEE) received the Ph.D. degree in physics from the Universitat Autónoma de Barcelona (UAB), Bellaterra, Spain, in 1992.

She is currently a Full Professor with the Department of Electronics Engineering, UAB. She has been working for the past 20 years in the field of micro-electromechanical systems (MEMS) resonators and their integration within CMOS technologies focused on the reduction in dimensions toward nanoelectromechanical devices with optimized CMOS conditioning circuitry. She has coauthored more than 100 research articles and 200 peer-reviewed conferences. Her research interests include the study of novel piezoelectrical micro/nanometric ultrasonic transducers, their integration with CMOS toward efficient biometrics systems, and exploitation of nonlinear NEMS resonators.

Dr. Barniol was a recipient of the Award of the Universitat Autónoma de Barcelona, for Research Excellence in the area of Technology, in 2009. She has been on Program Committee of several conferences, including IEEE-IEDM, IEEE-MEMS, MNE, Transducers, and Eurosensors.